

Document downloaded from:

<http://hdl.handle.net/10251/204084>

This paper must be cited as:

Serrano, J.; Piqueras, P.; Angiolini, E.; Garcia-Afonso, O. (2023). Fuel economy benefits in internal combustion engines due to soot restructuring in the particulate filter by water injection. *International Journal of Engine Research*. 24(4):1630-1642.

<https://doi.org/10.1177/14680874221099898>



The final publication is available at

<https://doi.org/10.1177/14680874221099898>

Copyright SAGE Publications

Additional Information

This is the author's version of a work that was accepted for publication in *International Journal of Engine Research*. Changes resulting from the publishing process, such as peer review, editing, corrections, structural formatting, and other quality control mechanisms may not be reflected in this document. Changes may have been made to this work since it was submitted for publication. A definitive version was subsequently published as <https://doi.org/10.1177/14680874221099898>.

Fuel economy benefits in internal combustion engines due to soot restructuring in the particulate filter by water injection

José Ramón Serrano¹, Pedro Piqueras¹ ,
Emanuele Angiolini¹  and Óscar García-Afonso² 

Abstract

Wall-flow particulate filters are key elements to control particulate matter emissions. The stricter emission standards also for non-road mobility machinery makes this device essential to improve the air quality in the short to medium term. However, their high filtration efficiency brings with it an increase in backpressure. This effect becomes more damaging as particles get accumulated in the filter and in hybrid vehicles where exhaust temperature are lower due to more frequent cold starts. Pre-filter water injection is a proven method to reduce the impact of soot load on the pressure drop avoiding the fuel consumption increase. In this paper, the effect of pre-filter water injections is analysed in engine and flow test rig environments. After verifying the impact of consecutive injection events on fuel consumption, the filter was loaded and divided into quarters. These were studied one at a time in flow test rig to separate soot mal-distribution from water drag effects. A wide range of conditions were tested to assess the change in pressure drop generated by a single injection. With this reference, the soot restructuring pattern was analysed employing optical techniques. These provided evidences of the way the soot fragments got released from the particulate layer and moved towards the inlet channels rear end. Additionally, a closer look into the porous wall micro-structure provided insights explaining the lack of effect on filtration efficiency. These results provide a basis for synergistic removal of vehicle condensates for use in fuel consumption reduction.

Keywords

CO₂ emissions, internal combustion engines, particulate matter, particulate filter, water injection, pressure drop

Introduction

Particulate matter, one of the main pollutants of internal combustion engines,¹ has adverse effects on human health causing cardiovascular and respiratory diseases.² Despite the efforts to control engine-out particle emissions, the use of wall-flow particulate filters (PFs) has become the only viable and reliable way to fulfil the emission regulations for automotive, commercial and off-road machinery.^{3–5}

Wall-flow PFs consist of axial parallel channels alternatively plugged at each end. This pattern defines the operating principle, forcing the exhaust gas to pass through a porous wall where particulate matter is filtered. As a result, the accumulated particle matter produces a pressure drop increase. This behaviour has a negative impact on the fuel economy⁶ and becomes

more detrimental as soot and ash are collected.⁷ Only limited engine operating conditions allow the exhaust flow to reach enough temperature and NO₂ content to promote the soot oxidation and lead the filter to a low pressure drop equilibrium condition.⁸ Therefore, frequent events of forced soot oxidation are required to control the PF backpressure and avoid uncontrolled

¹CMT-Motores Térmicos, Universitat Politècnica de València, Valencia, Spain

²Departamento de Ingeniería Industrial, Escuela Superior de Ingeniería y Tecnología (ESIT), Universidad de La Laguna (ULL), La Laguna, Tenerife, Spain

Corresponding author:

Pedro Piqueras, CMT-Motores Térmicos, Universitat Politècnica de València, Camino de Vera s/n, Valencia 46022, Spain.

Email: pedpicab@mot.upv.es

regenerations with a consequent hardware failure.⁹ The common approach to trigger the soot oxidation is a late fuel injection, resulting in an additional source of fuel consumption,¹⁰ emissions¹¹ and oil dilution.¹² This problematic becomes notorious in modern engines, as soot engine-out emissions increase due to the high level of exhaust gas recirculation rates required to reduce NOx emissions.¹³ In gasoline engines, the soot oxidation, and hence the pressure drop during real driving conditions, is dependent on fuel cut-off events.¹⁴ In addition, the ash accumulation in the inlet channel along the PF lifetime deteriorates the fuel consumption and causes on-board control issues.¹⁵

Data reported in the literature has shown fuel consumption penalties from imperceptible to a maximum of 1.3% in lab-test type driving cycles for different filter substrates.¹⁶ From the ash accumulation point of view, Zhang et al.¹⁷ reported ash induced fuel penalty typically ranging from 0.02% to 0.42% whilst Jang et al.¹⁸ reported up to 5% of fuel penalty in aged filters under the FTP-75 driving cycle. Alternatives to the common square channels have been proposed to reduce the fuel penalty, such as asymmetric geometry with larger inlet than outlet channels of different geometries.^{19,20} Coated particulate filters are also emerging, with additional concerns on pressure drop.^{21,22}

Deposits structure plays a key role in the pressure drop and soot/ash load relationship.¹⁷ Techniques able to restructure the layer into a plug contribute to improve the fuel economy by reducing the backpressure and extending the interval between active regenerations. To the best of author's knowledge, there are OEMs studying the pre-PF water injection with off-board water supply.²³ With a similar approach, on-board pre-PF water injection²⁴ has been proven as a robust and effective method to reduce soot-loaded PF pressure drop.^{25,26} As a proof of concept, Bermúdez et al.²⁷ performed soot loading processes that revealed that this technique allows a filter backpressure control even under extreme soot levels. To achieve such control, multiple water injections were necessary. Although the study did not cover an exhaustive investigation of the injection system, a minimum injected water quantity of 200 g and 66 g/s in every injection were required to effectively limit the pressure drop increase, corresponding to an average water consumption of 0.23 kg/h in NEDC operating conditions. A benefit of 1% in fuel consumption was found at the low demand driving cycle NEDC. Better fuel economy numbers would be expected in driving cycles such as WLTC or US06 where the power demand is higher. Besides the water injection rate, the period between injection events played a key role to keep the pressure drop below a certain limit. A clear decay in the injection effectiveness with the number of injection events was found, finding the initial ones the most effective. This result pointed out the need for robust control strategies maximising the benefits between target pressure drop, delay in active regeneration and injection cost. Besides

performance analysis, experimental results²⁷ revealed the lack of impact on tailpipe particle and gaseous emissions during the water injection events.

This first experimental work showed the soot restructuring as a potential cause of the benefits from pre-PF water injections keeping constant the filtration efficiency and active regeneration capability. However, modelling results²⁸ evidenced a lower soot oxidation rate in the rear-end zone when pre-PF water injections were previously applied. The entering and middle regions of the inlet channels were regenerated very fast making the pressure drop rapidly decrease. However, the rear end region of the inlet channels behaved as a plug end. As a consequence, the filtration velocity, that is, the mass flow, was very low along this region. Therefore, the soot oxidation became limited by mass transfer. This kind of response might induce partial regenerations, which should be avoided for long-term benefits from pre-PF water injection. Optimising the regeneration strategy is mandatory to avoid partial oxidation and, therefore, maximise the benefit in fuel economy that this method brings. In fact, despite these needs and the fact that the limit for maximum soot load still exists because of the risk of uncontrolled regenerations, the results obtained in all these works show the potential benefits to control the trigger for a more effective active regeneration. It should depend on soot loading criteria only but not on pressure drop concerns affecting negatively the fuel consumption. In addition, the impact of ash along the filter lifetime would be reduced by its active restructuring in the inlet channels rear ends bringing similar pressure drop reductions as that obtained for soot accumulation.

The aim of the present paper is to complement the aforementioned research works from the component point of view. Thus, the study was focussed on in-situ optical analysis of the soot restructuring in the channels after injection events complemented by the performance metrics based on pressure drop reduction. These results provide an insight of the root cause causing the experimental and computationally proved pressure drop reduction.

Background on soot and ash deposition effect on pressure drop

The deposition in the filter can be divided into two main stages: deep bed filtration and cake filtration.²⁹ In the first stage, the pores of the substrate get filled with soot causing a change of the wall micro-structure. Characterised by low soot penetration, as concluded from experimental³⁰ and modelling approaches,³¹ this phase results in a rapid pressure drop increase.³² The wall porosity does play a key role during this phase, as high-porosity substrates can contain more soot in their pores and cause a less prominent pressure drop increase.³³ The soot then starts building a layer up on top of the porous surface leading to the cake filtration

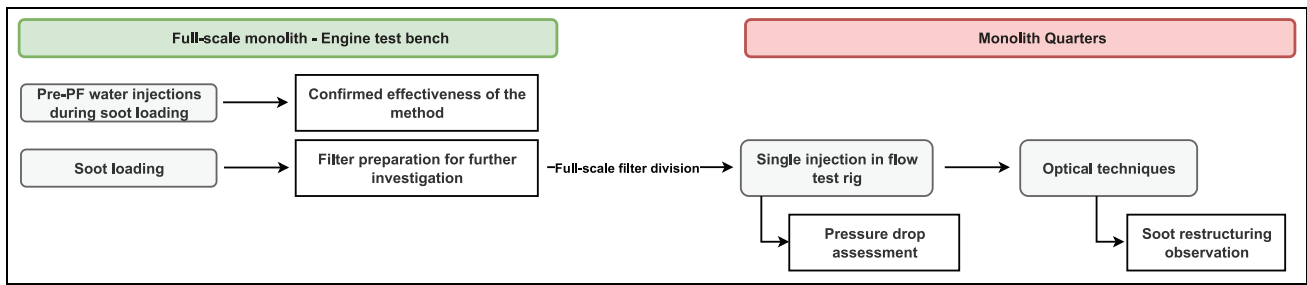


Figure 1. Scheme of the research methodology.

regime.³⁴ This phase is characterised by a moderate pressure drop increase, with a common nearly constant rate set by the soot layer properties. Once reached high levels of soot load, the result is a soot layer with an almost constant thickness along the filter channels.³⁵

The inorganic matter bound to the soot particles also accumulates inside/on the porous wall and as end-plug in the inlet channels. The ash deposition inside the porous wall takes place mainly at the beginning of the filter lifetime. Although the proportion of ash in this location is much lower than the others, its contribution to the ash induced pressure drop may reach up to 50%.³⁶ The origin of ash deposits is related to the soot layer oxidation. During this process the soot gets broken into pieces, leaving ash fragments when the soot is completely burned.³⁷ These fragments form a semi-uniform layer on top of the surface or are pushed back to the rear end by the flow. Regeneration strategies³⁸ and ash stickiness³⁹ are the most important aspects governing the ash layer to plug ratio. In addition, aged PFs might present mid-channel ash plugs,³⁸ what causes an excessive pressure drop.

Data reported in the literature show that a low amount of ashes has a positive impact on pressure drop during soot loading with respect to a fresh filter. The reason resides in the fact that the formed ash layer restricts the deep bed filtration,^{15,40} in the same way heterogeneous porous wall emulates.⁴¹ However, this benefit vanishes as ash accumulates over the filter lifetime. The ash plug length increases and the effective volume decreases, what shortens the filter soot capacity¹⁵ and increases the pressure drop.⁴² Although the ash layer to plug ratio plays an important role on the filter backpressure, there is not a conclusive answer regarding the optimum ratio. However, the typical low permeability of ash makes that a reduction in pressure drop is found if end-plug is the prevalent deposition.⁴³ These topics raise the interest for technologies to control the soot and ash distribution, like deposits mobility based on pre-filter water injection. This technique consists of pressurised water injected upstream of the filter when a threshold in pressure drop is reached. The water stream in the inlet channels modifies the soot layer structure pushing the soot back to the rear part of the inlet channels, as Scanning Electron Microscope (SEM) analysis and modelling techniques has previously

shown.²⁸ As a result, the overall filter pressure drop is reduced, improving the engine thermal efficiency.

Experimental setup and research methodology

The pre-PF water injections alter the soot particle deposition leading to the reduction of the pressure drop across the filter.²⁵ With this objective in mind, the experimental method described in Figure 1 has been designed. In a first instance, a full-scale filter testing phase in engine test bed was performed. These tests provided simultaneously the required soot load in the filter and the confirmation of the water injection effectiveness. The second stage in the methodology comprised the division of the full-scale loaded monolith into quarters for further investigation in a flow test rig. By applying one single injection in an accurate-controlled environment, it was possible to quantify the water injection effect as function of gas mass flow and temperature. As a final step, the quarter samples were analysed with SEM and microscope to gather evidences that explain how the soot is restructured after an injection event.

PF description and quarter samples preparation

The main characteristics of the wall flow PF used in this study are summarised in Table 1. Once the testing phase with the full-scale PF ended, the monolith was mechanically extracted from the canning with a press and divided into four quarters. Every sample was placed back into the canning, modified as shown in Figure 2. The support was sealed and mounted in the flow test rig to measure the pressure drop generated by every quarter sample.

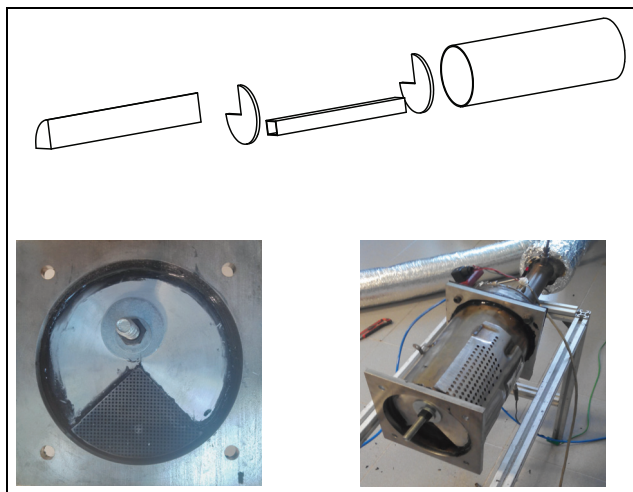
Engine test bed

The PF was loaded in a 1.4L Euro5 passenger car Diesel engine installed in a test bed equipped with a dynamometer controlling engine speed and torque. The engine characteristics are summarised in Table 2.

Figure 3 shows the engine test bed schematically. The production engine hot-end was modified to allow pre-PF water injections. This system was based on a

Table 1. Characteristics of tested PF.

Diameter (mm)	140
Length (mm)	230
Plug length (mm)	5
Volume (l)	3.46
Cell width (mm)	1.423
Wall thickness (mm)	0.458
Cell density (cps)	180
Porosity (-)	0.41
Mean pore diameter (μm)	18.55

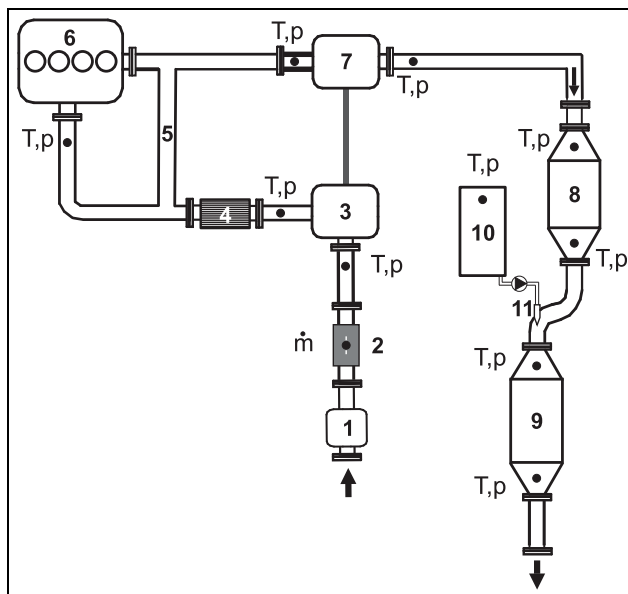
**Figure 2.** Scheme and pictures of the support for quarter filter samples tested in the flow test rig.

pressurised water tank at 5 bar coupled to a 4 mm diameter nozzle placed in the inlet canning cone. The injected water mass was controlled by means of an electronic valve governed by an analogical timer. This setup provided an injection rate of approximately 84 g/s, above the minimum threshold of 66 g/s identified in the work of Bermúdez et al.²⁵ as a required rate. Although the injection system was simple, it was proven to be effective for pressure drop control proposals and repeatable.²⁵ Despite a preliminary study dealing with the influence of the injection rate and the amount of injected water,²⁵ the water stream characteristics, such as droplets size distribution or radial uniformity, were not analysed. Although these features could play a relevant role in terms of cost and contribute to decreasing the required amount of water or the frequency of the injection events, their optimisation was kept out of the scope of this work.

To avoid passive soot oxidation by NO_2 , which would reduce the soot load increasing rate, the oxidation catalyst was removed during the loading processes. Besides the NO_2/NO_x ratio in the exhaust gas stream, this decision could also impact on the nature of the collected particulate matter. In this regard, the experimental results regarding the use of pre-PF water injection shown in previous works were obtained with an

Table 2. Engine specifications.

Type	Passenger car diesel engine
Injection system	Common-rail
Turbocharger	VGT
Displacement	1461 cm^3
Bore	76 mm
Stroke	80.5 mm
Cylinders number	4
Valves number	4 per cylinder
Compression ratio	1:15.3
Maximum power	77 kW at 4000 rpm
Maximum torque	240 Nm at 2000 rpm

**Figure 3.** Scheme of the engine test bench. (1) Air filter. (2) Hot wire flow metre. (3) Compressor. (4) Cooler. (5) HP EGR line. (6) Engine. (7) Turbine. (8) Dismountable DOC. (9) PF. (10) Pressurised water tank. (11) Water injector.

oxidation catalyst placed upstream of the filter. Although these studies were not focussed on the impact of the oxidation catalyst and the tests were done in a different engine than the one used in this work, the response obtained with and without catalyst was very similar. Therefore, the presence of the oxidation catalyst did not affect the core of the discussion. Every time the filter had to be actively regenerated the catalyst was mounted again and a post-injection was imposed.

Figure 3 also includes the air-path instrumentation. Black dots indicate the measurement location. Focussing on the filter, both inlet and outlet temperature and pressure were measured. Engine performance magnitudes were also measured: temperature and pressure along the air path, air and fuel mass flow, engine speed and torque. The sensor types, measurement ranges and accuracy of the instrumentation are included in Table 3.

Table 3. Characteristics of the test bench instrumentation.

Magnitude	Sensor	Range	Accuracy
Air mass flow	Sensyflow	0–720 kg/h	±1% (actual value)
Fuel mass flow	Gravimetric balance	0–27 kg/h	±0.12% (full-scale)
Mean pressure	Piezoresistive PMA P40	0–6 bar	±0.3% (full-scale)
Temperature	Type K thermocouple	–200°C to 1200°C	±1°C or 0.4% (actual value)
Torque	Torquimeter	–650 to 650 Nm	±0.1% (full-scale)

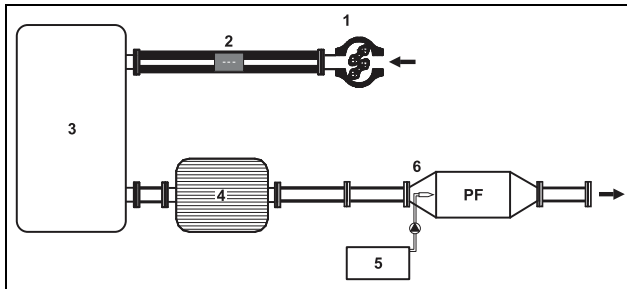


Figure 4. Scheme of the flow test rig. (1) Roots blower. (2) Hot wire flow metre. (3) Settling chamber. (4) Electric heater. (5) Pressurised water tank. (6) Water injector.

Hot flow test bench

The pressure drop of the quarter samples was measured at different air mass flow and temperature in the hot flow test rig described in Figure 4. Ambient air was forced to flow through the sample by means of a roots-type compressor. An electrical heater was placed upstream of the tested element. The pressure drop was measured in each quarter sample at cold and warm conditions. The flow temperature was controlled with a PID, connected to a thermocouple at the PF inlet, that regulated the electric heater power. The air mass flow was monitored with a hot wire flow metre mounted upstream of the settling chamber. The filter pressure drop was measured with a water/mercury column in case of low/medium or high pressure drop respectively. Every tested point was recorded once the thermal transient ended, that is, when the outlet PF temperature reached a stationary value.

Optical techniques

A scanning electron microscope was used to conduct the optical analysis of the quarter samples after pre-PF water injections in the flow test rig. A JEOL JSM-6300 SEM with X-rays analyser was used coupled to the INCA software of Oxford Instruments for data acquisition and post-processing.

The data extracted from SEM was complemented with macroscopic information from a PCE-MM200 digital magnifier. This device provided images up to 200 magnification, that is, of the order of magnitude corresponding to the monolith cell dimension. The magnifier was mounted on a guide rail connected with

two digitally controlled actuators that allowed the precise motion of the magnifier in two directions, covering the whole cross-section area of the monolith.

Test campaign description

This section covers a detailed description of each test performed in engine and hot flow test benches in chronological order.

Pre-PF water injections in engine test bench. The objective of this test was to confirm previous experimental evidences,²⁸ measured with different hardware than the one in the current research, demonstrating the effectiveness of the pre-PF water injection and the applied setup. An steady-state operating point corresponding to 2250 rpm and 50 Nm was chosen to load the PF. The injected fuel mass was kept constant during the entire soot loading test. Across the entire soot loading test, 22 water injections took place upstream of the PF. The first injection started at a filter soot load of 12.6 g (3.6 g/l), corresponding to a pressure drop of 4 kPa. This is a soot load typically below the threshold to trigger active regenerations. The test ended with a PF soot load of 49.6 g (14.3 g/l). Therefore, the wide range of soot load in which water injections were applied shows the potential of the technique to reduce the penalty in fuel consumption from loaded PFs whilst the active regeneration trigger might be set from soot mass-based criteria instead of pressure drop concerns, which can be highly related to the engine operating conditions. During this test, the injector was opened for 2 s. As a result, 168 g of water per event was injected. The mean time between injections was 19 min, what meant approximately 530 g/h of water consumption.

Reference soot loading in engine test bench. After an active regeneration, the PF was loaded again without pre-PF water injections. The same engine operating point and settings were used. After this test, the PF with a soot load of 44.6 g (12.9 g/l) was divided into four identical quarters.

Single pre-PF water injection in flow test rig. After weighting the four samples, the pressure drop of each sample was measured in the hot flow test rig. Two targets of pre-PF inlet gas temperature were chosen: 20°C and 200°C.

Table 4. Performed injections for every quarter sample in the flow test rig.

Quarter	Air mass flow (kg/h)	Inlet temperature (°C)	Injection pressure (bar)	Injector opening time (s)	Water mass flow (g/s)	Injected water mass (g)
#1 Ref	–	–	–	–	–	–
#2	35	200	5	2	84.3	168.6
#3	20	200	5	2	85.3	170.6
#4	20	200	5	1	83.2	83.2

Higher temperatures were not considered to avoid undesired soot oxidation. For both temperatures, the roots blower power was gradually increased to raise the air mass flow and then decreased again to measure the pressure drop of every quarter sample twice. In this way, any change in pressure drop due to compressibility of the soot cake was discarded.

After the pressure drop measurements, three out of four quarter samples were subjected to a single pre-PF water injection. The water supply system used in the engine was installed in the flow test rig. The injections were performed at 200°C in gas temperature, representative of low-demanding urban driving cycles. To avoid the effect of the cooling (water at room temperature) on the pressure drop, measures were taken after the monolith thermal transient was completed. Finally, the samples were weighted again to confirm the avoidance of soot release due to the injection.

Table 4 summarises the injection settings for each quarter sample. The differences in mass flow and water injected allow to check the sensitivity of pre-PF water injections efficiency to these parameters:

- Quarter #1: no water injection (reference).
- Quarter #2: 168.6 g of water in 2 s; air mass flow set to 35 kg/h.
- Quarter #3: 170.6 g of water in 2 s; air mass flow set to 20 kg/h.
- Quarter #4: 83.2 g of water in 1 s; air mass flow set to 20 kg/h.

Results and discussion

The experimental information gathered allowed a deep analysis of the pre-PF water injection effect on the filter backpressure. First, the results of consecutive pre-PF water injections during soot loading in engine provides data to judge the benefits of this technique from a system level point of view, as previously shown in Bermúdez et al.²⁵ The second group of results is focussed on the understanding of how the soot is restructured in the monolith channels.

Engine test bench injections analysis

Figure 5(a) shows a comparison of the pressure drop evolution during a soot loading test between reference

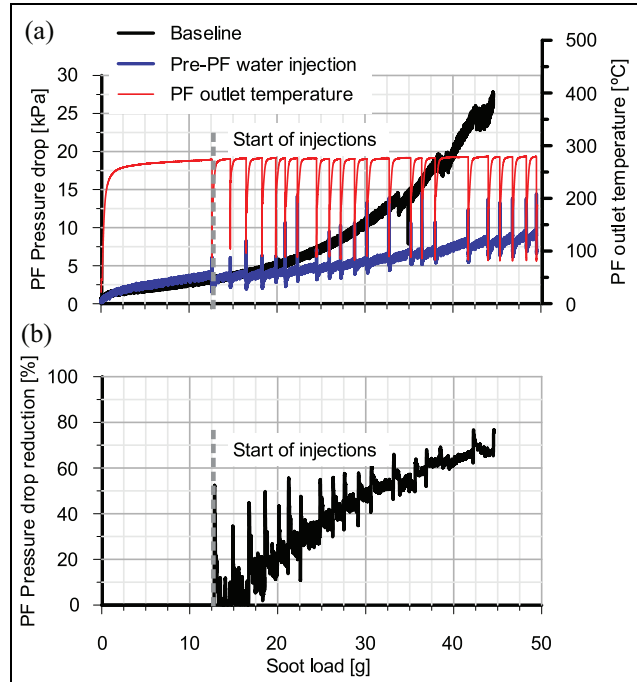


Figure 5. Comparison of pressure drop with and without the pre-PF water injection technique during the soot loading test: (a) Pressure drop evolution and (b) Pressure drop reduction due to pre-DPF water injection.

(black line) and applying pre-PF water injections (blue line). As stated in Bermúdez et al.,²⁵ the PF outlet temperature (red line in Figure 5(a)) shows that the pressure drop reduction is not caused by the monolith cooling induced by water injections. The thermal transient duration after every injection is short compared to the interval between injections. Once the outlet temperature recovers its nominal value, the pressure drop reduction is evident compared to the reference test.

As the soot loading progresses, the pressure drop reduction due to water injections becomes noticeable, as Figure 5(b) depicts. The reduction raises from 10% after the first injection to 70% at the end of the test. Although the pressure drop was not kept constant, a noticeable reduction in the order of 17 kPa compared to the reference was achieved.

Figure 6 shows the engine performance during both tests, which were carried out at constant pedal. The VGT rack position remained also constant through the test leading to an approximately constant expansion

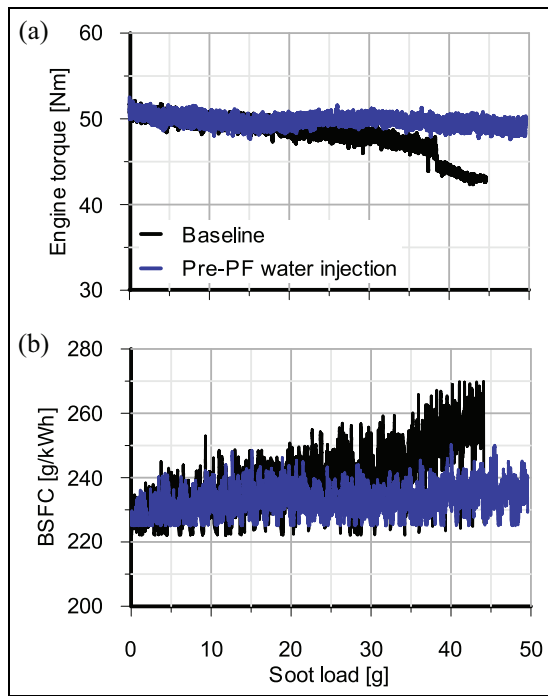


Figure 6. Engine performance during the soot loading test with and without pre-PF water injections: (a) torque and (b) BSFC.

ratio. Pre-PF water injections present a clear advantage in reducing the pumping losses, what results in a less pronounced decay of the engine torque, as Figure 6(a) shows. The fuel economy benefit applying this technique can be extracted from the engine brake specific fuel consumption (BSFC) showed in Figure 6(b). Benefits of 2.5%, 4% and 8% were obtained at soot loading levels of 5, 8 and 12.8 g/l, respectively. These results confirm the validity of this technique to control the engine backpressure, as previously pointed out in Bermúdez et al.²⁵

Flow test rig injections analysis

As described before, every quarter was measured twice in the hot flow test rig performing an air mass flow sweep between 5 and 35 kg/h. The comparison of the pressure drop before and after the water injection is shown in Figure 7. Each row corresponds to each quarter sample. Plots on the left refers to 20°C inlet gas measurement while the right ones include data at 200°C. The good repeatability between the pressure drop measurements before and after water injection guarantees that the increasing inlet pressure did not cause any particle layer detachment or compression. These results allow a good analysis of the pre-PF water injections impact with confidence.

The differences in the maximum air mass flow reached for each sample are explained by the root blower limitations to provide the desired mass flow when the pressure drop is high, especially in hot tests. A variability of the quarter pressure drop before the

injection is observed. Quarters #1 and #3 present the highest pressure drop, followed by quarters #4 and #2. This behaviour is supposed to be related to soot maldistribution inside the filter.

The clear difference between quarters pressure drop before and after water injections confirms the effectiveness of the technique. Pressure drop reductions in the range of 75%–90% were observed in the three samples. These values are in the same order of magnitude than the ones showed in Figure 5 (full-scale monolith) for the maximum soot load. The results indicate that the quarter #4, with half of water mass injected according to Table 4, produced the minimum benefit. This evidences the limited effect of the mass flow during the injection, being the water mass the dominant parameter. However, the limited number of samples did not allow running a wider design of experiments avoiding a deeper analysis of the water injection settings and flow conditions impact on the effectiveness of this technique.

Optical description of soot restructuring

Each quarter sample was cut in five sections at 0, 2.5, 8.5, 14.5 and 20.5 cm from the inlet frontal section. Following the nomenclature shown in Figure 8 (to be used hereafter), 17 pictures of the inlet and outlet faces of each section were taken resulting in 170 pictures available per quarter sample.

The water stream pushes the soot cake towards the end of the channel, as it can be observed in Figure 9 that shows images of the second section (2.5 cm from the sample inlet) of each quarter sample. Figure 9 also includes three images taken with the optical microscope corresponding to positions 1, 11 and 13 (nomenclature in Figure 8). The high amount of soot was almost completely blocking the inlet channel of the reference sample (no water injection). By contrast, the samples subjected to pre-PF water injection show zones with unblocked inlet channels, corresponding to areas reached by the water stream.

This fact is related to the injection setup. The water injection was performed using a simple nozzle, unable to generate a water spray homogeneously distributed throughout the quarter sample frontal section. To overcome this problem, the injector was mounted in the manner that the water stream hit in the first place the metallic cover of the support (Figure 2). The generated water droplets fall down by gravity and were made to flow in the quarter by the inlet air flow drag. This leads to conclude that optimising the injector geometry to affect the whole frontal section is a key feature to reach higher benefits. Although a relevant further reduction in pressure drop is not expected (currently ranges 75%–90%), an injection optimisation would lead to a more homogeneous distribution of de-clogged channels. This behaviour would mean better distribution of the new soot being filtered leading to a lower rate of pressure drop increase. Hence, longer intervals between injections (less water consumption) would be needed.

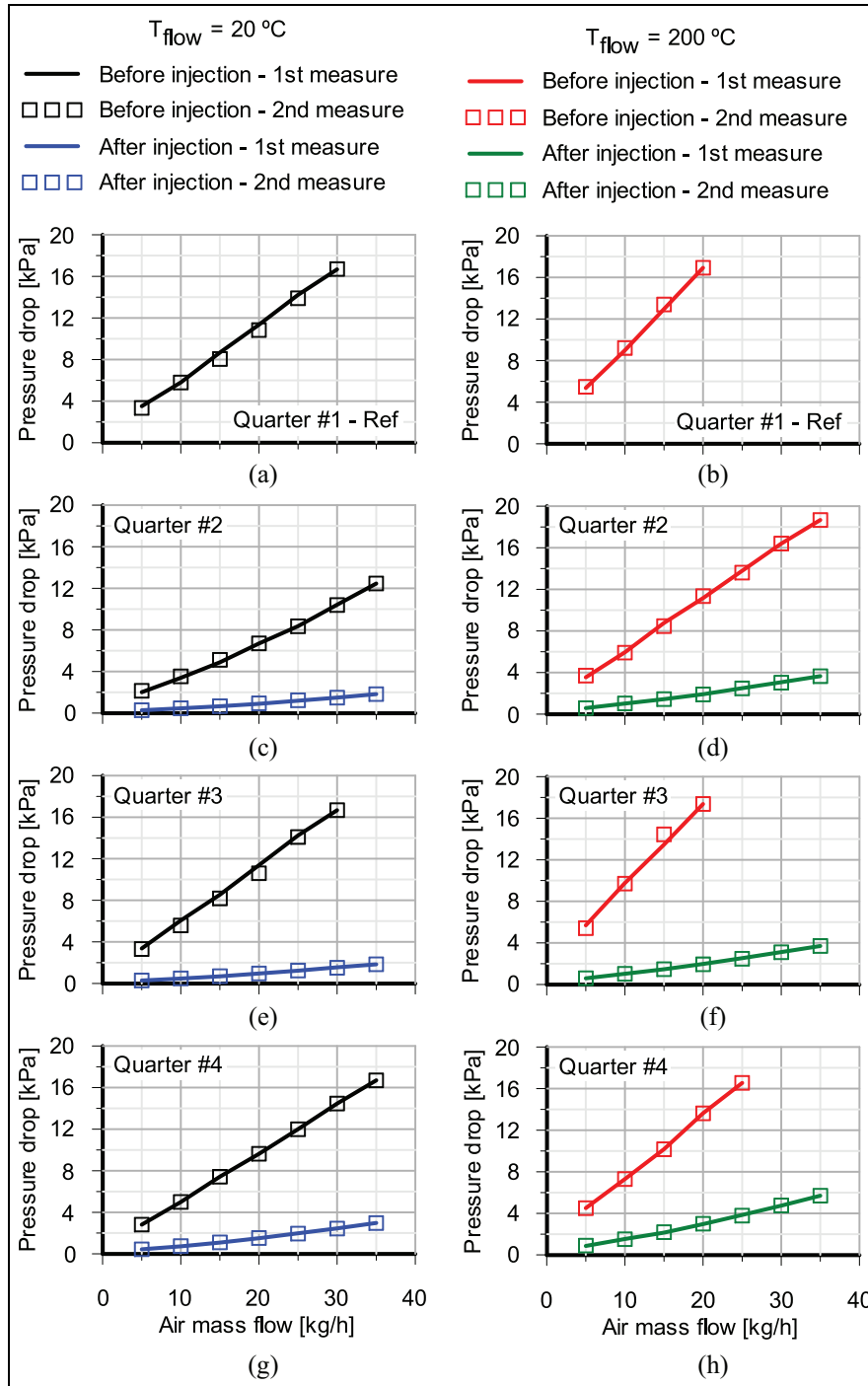


Figure 7. Monolith quarter samples pressure drop as a function of air mass flow and inlet temperature before and after pre-PF water injection: 20°C in quarters (a) #1, (c) #2, (e) #3 and (g) #4, and 200°C in quarters (b) #1, (d) #2, (f) #3 and (h) #4.

Microscope image post-processing determined the mean soot layer thickness distribution along the inlet channels. Figure 10(c) shows the result for the reference quarter (#1) as function of the axial position. Coloured pictures (Figure 10(a)) to black and white where white spaces identify soot free regions, as Figure 10(b) shows. If the clean cell size is known, the calculation of the white spaces area provides the average layer thickness. For every axial position, four images of the central part of the sample were analysed: positions 7, 8, 11 and 12.

As shown in Figure 10, every picture contains six channels. Figure 10(c) shows the result for the reference quarter (#1) as function of the axial position. Coloured symbols represent the mean values for every cross-section position, while vertical bars show maximum and minimum interval of estimated layer thickness. The large variability and the absence of axial trend evidences an almost constant particle layer thickness along the filter channel, with a value comprised between 500

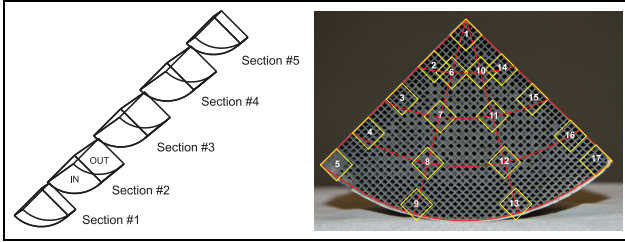


Figure 8. Scheme of the different sample sections and pictures code.

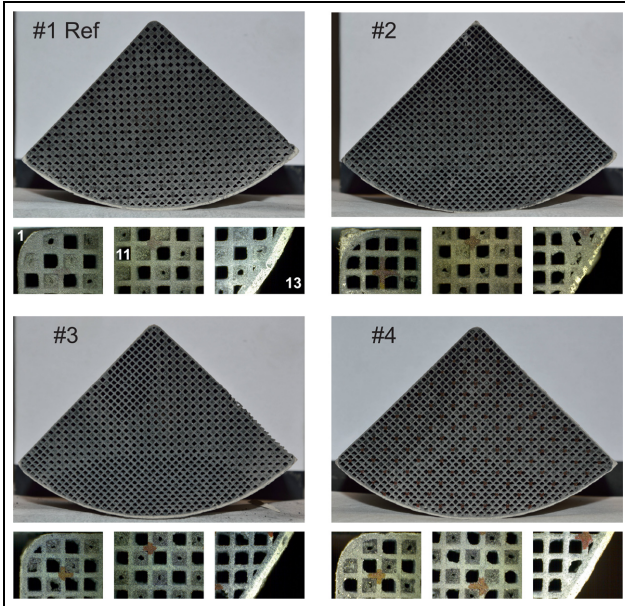


Figure 9. Camera and optical microscope pictures at Section #2 of each quarter sample.

and $600\ \mu\text{m}$. Also Koltsakis et al.³⁵ and Lupše et al.⁴⁴ reported axial uniform particle layer thickness for high PF soot loads.

Considering an almost constant soot layer thickness along the channel, any change shown by the microscope will be related to the pre-PF water injection. In order to analyse the samples subjected to water injection, an approach based on the post-processing of section pictures along the quarter’s length was proposed. The two-colours technique was applied to each quarter sample to quantify the number of channels that were de-clogged by the water stream. First, every picture was passed to black and white colours where white regions represents an open channel for both inlet and outlet (except the ends of the quarters where plugs are visible). Therefore, extremely clogged inlet channels are identified by a very small white region, as Figure 11(a) depicts. Afterwards, the code compares the area of every white region with a threshold value representative of a clean channel. If this is the case, the code plots a red cross at the centroid of the white square (Figure 11(b)). The

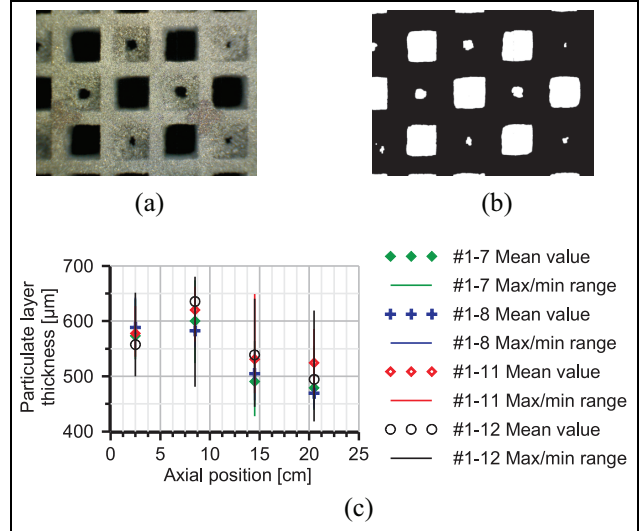


Figure 10. (a) Original microscope picture, (b) black and white picture after post-processing and (c) particle layer thickness as a function of the axial position for quarter sample #1 (Reference).

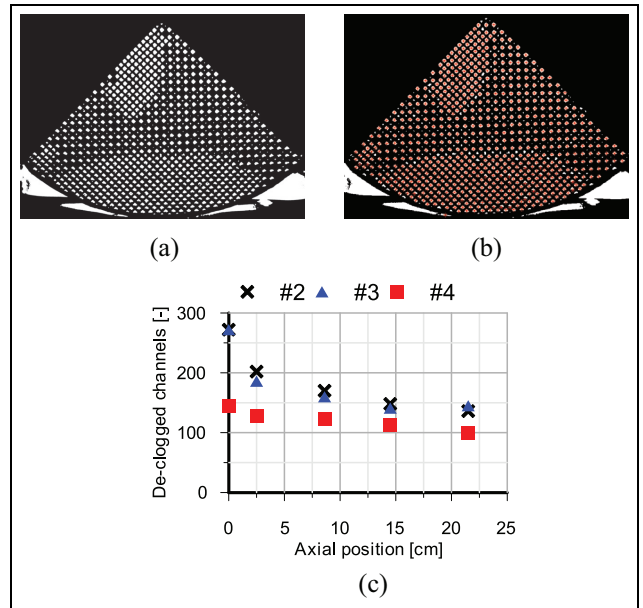


Figure 11. (a and b) Post-processing for open channels count and (c) number of de-clogged channels as a function of the axial position for the quarter samples subjected to pre-PF water injection.

number of de-clogged channels is obtained by subtracting the known outlet channels number to the counted clean channels.

Figure 11(c) shows a summary of the results along the three quarter samples subjected to water injection. The plot clearly shows that the number of de-clogged channels decreases with the axial position, that is, as the water droplets penetrates into the sample. Quarter #4 had the smallest number of de-clogged channels.

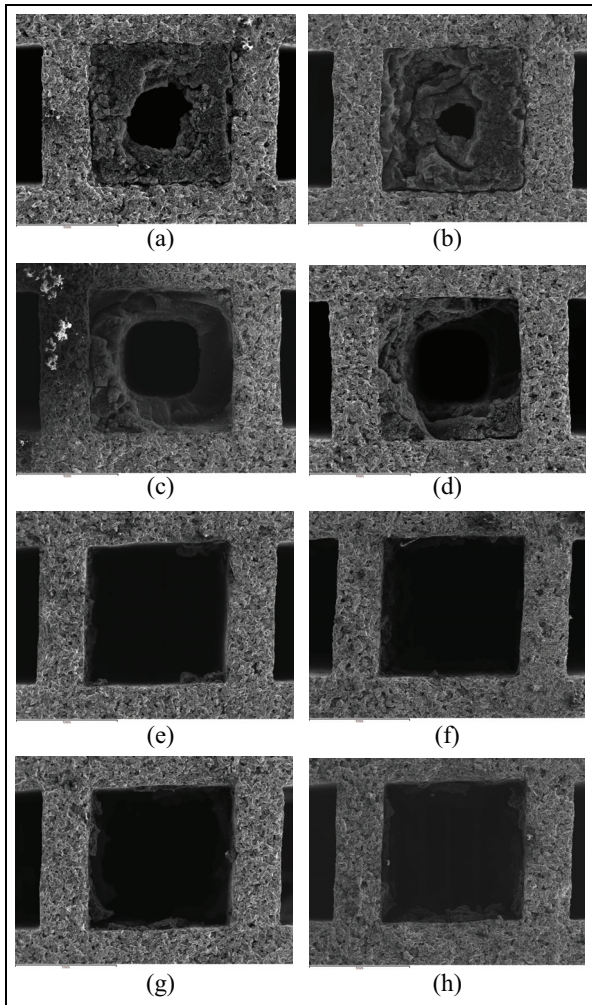


Figure 12. SEM images of reference and #3 quarter sample at 2.5 and 20.5 cm from the inlet section: (a) #1 Ref – 2.5 cm, (b) #1 Ref – 2.5 cm, (c) #1 Ref – 20.5 cm, (d) #1 Ref – 20.5 cm, (e) #3 – 2.5 cm, (f) #3 – 2.5 cm, (g) #3 – 20.5 cm and (h) #3 – 20.5 cm.

This result also agrees with the higher pressure drop after the water injection compared to quarters #2 and #3, as shown in Figure 7. Quarters #2 and #3 presented similar number of de-clogged channels as well as similar pressure drop after the injection. The slight differences between these two quarters might be related to the higher air mass flow during the injection in quarter #2, what results in higher droplets momentum, hence higher penetration and drag capacity.

A more detailed visual inspection was possible using SEM. It allows a deeper understanding of the water flow effect on the particle layer and evaluate if the water injection affected the soot deposits inside the porous wall. The use of X-rays analyser also allowed a precise distinction of monolith porous wall (SiC) and soot particles (C). The samples for SEM analysis were taken in the lower external part of the quarters since this was the most affected area by the water flow in all three samples subjected to pre-PF water injection, as Figures 9 and 11 previously demonstrated.

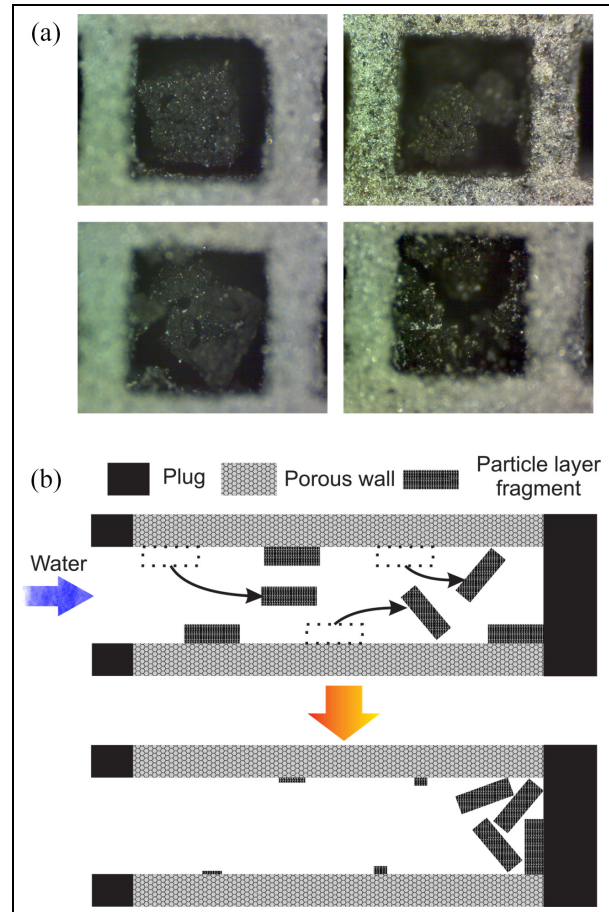


Figure 13. (a) Optical microscope images of fragments of particle layer accumulated in the rear end part of the inlet channels and (b) scheme of the water effect on particle layer fragments.

Figure 12 shows a comparison between the reference quarter sample #1 (not subjected to water injection) and the quarter #3 at two axial positions: 2.5 cm (front section) and 20.5 cm (rear section). The reference case shows a thick particle layer, slightly thinner in the rear section. On the contrary, the soot layer in sample #3 was strongly modified by the water injection. The thick layer in the front section turned into a thin layer covering the channel surface with sparse, random presence of soot. It resulted in a maximum thickness of $130\ \mu\text{m}$, five times lower than the reference one. The presence of soot slightly increases in the rear part of the channels. In this region, the maximum measured particle layer thickness goes from the 130 to $180\ \mu\text{m}$. Nevertheless, this value is still notably lower than the layer thickness of reference sample at the same axial position.

An additional cut was performed at 21.5 cm from the inlet frontal face to provide further information of the soot layer structure near the rear end plug. Views from several channels are showed in Figure 13(a). The accumulation of big layer fragments (in dark colour) is evident. This result indicates that the water flow tends to detach fragments of the particle layer and push them towards the end of the inlet channels. Figure 13(b)

sketches the hypothesised effect of the water streams on the soot layer. This hypothesis is further supported by the observed different adhesion of the particle layer in channels affected or not by the water injection. The particle layer was firmly stuck on the porous wall in the channels, not affected by water injection. By contrast, channels affected by the water injection presented a particle layer weakly stuck on the porous wall.

The images also provided valuable information about the impact of water injections on the soot particle deposits inside the porous wall. Figure 14 provides a detailed view of the soot layer of quarter samples #1 and #3 at 2.5 and 20.5 cm from the frontal face. The elemental analysis of the samples is also shown, with the presence of Silicon, that is, monolith porous wall grains, marked in green and Carbon (soot) in red. The well known superficial deposition of soot with negligible penetration inside the porous wall³⁰ regardless of the sample analysed (reference and with pre-PF water injection) is observed. In both cases, the pores are clean. Therefore, the water flow does not significantly affect the particles collected inside the porous wall. This evidence and the thin particle layer along the channel present after the pre-PF water injection justify the high filtration efficiency (>99%) measured by Bermúdez et al.²⁷ after the application of water injection.

Summary and conclusions

This paper presents a follow-up activity of previous research works regarding pre-PF water injection to control engine backpressure under medium-high levels of soot load. The new results confirmed the pre-PF water injection as an effective technique to reduce the pressure drop by means of altering the soot in-channel distribution. This has a positive effect on engine BSFC reduction, reaching in this work values up to 4% under the very representative 8 g/l of soot load commonly used as threshold to trigger an active regeneration.

The root causes of the observed pressure drop reduction have been identified by means of an in-situ optical analysis using a SEM and microscope. First, quarter samples of the full-scale filter were characterised in a hot flow test rig before and after a single water injection. This offered a direct indicator of pressure drop reduction. The samples were measured twice to confirm that the pressure drop difference was not related to soot layer density change. The water injection was performed with different air mass flow and injected water mass for each quarter sample. The quarter samples subjected to the single water injection showed a pressure drop reduction ranging from 75% to 90% for a 14 g/l soot load, similar to the outcome with the full-scale monolith in engine test bench. The results indicate that amount of water injected is the main parameter, obtaining positive effects as long as a minimum amount of water to produce soot drag is reached.

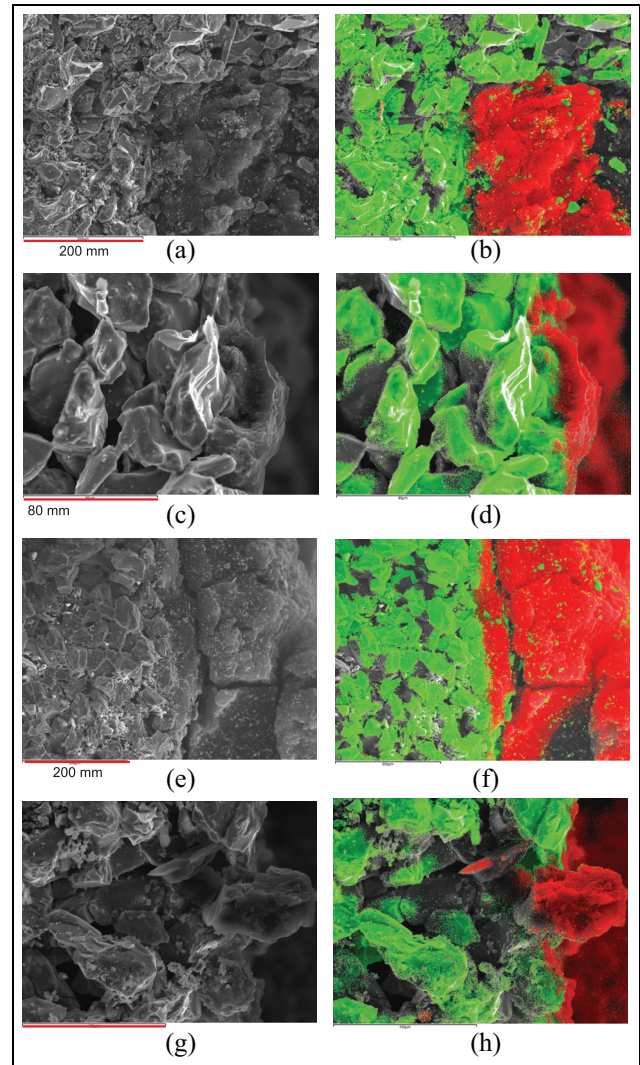


Figure 14. Examples of SEM images (left) and elemental map (right) from channels at different axial positions of quarter sample #1 (Ref) and #3: (a) #1 Ref – 2.5 cm, (b) #1 Ref – 2.5 cm, (c) #3 – 2.5 cm, (d) #3 – 2.5 cm, (e) #1 Ref – 20.5 cm, (f) #1 Ref – 20.5 cm, (g) #3 – 20.5 cm and (h) #3 – 20.5 cm.

Finally, the quarter samples were analysed with microscope and SEM. The information gathered revealed how the water flow in each channel pushes soot fragments back to the rear, getting stacked up in the channel rear end. The same behaviour was found in the three quarters subjected to water injections, although it seems less pronounced as the injected water mass was reduced. A negligible impact was observed on the in-wall soot deposits, what explains the previously measured high PF filtration efficiencies after the water injection.

The experimental results gathered from pressure drop measurement and in-situ soot restructuring observation have provided solid results confirming the noticeable benefits of this technique. However, additional topics such as the optimisation of the injection process, soot oxidation analysis in an extended range of operating conditions together with post-regeneration visualisation of the deposits in inlet channels or the

development and verification of a control strategy are worth to be studied further.

Declaration of conflicting interests


The author(s) declared no potential conflicts of interest with respect to the research, authorship, and/or publication of this article.


Funding

The author(s) disclosed receipt of the following financial support for the research, authorship, and/or publication of this article: This research has been supported by Grant PID2020-114289RB-I00 funded by MCIN/AEI/10.13039/501100011033.

ORCID iDs

Pedro Piqueras  <https://orcid.org/0000-0002-3767-0839>

Emanuele Angiolini  <https://orcid.org/0000-0002-9774-1344>

Óscar García-Afonso  <https://orcid.org/0000-0002-0946-1853>

References

- Joshi A. Review of vehicle engine efficiency and emissions. SAE technical paper 2020-01-0352, 2020.
- Kennedy IM. The health effects of combustion-generated aerosols. *Proc Combust Inst* 2007; 31: 2757–2770.
- Stamatellou AM and Stamatelos A. Overview of diesel particulate filter systems sizing approaches. *Appl Therm Eng* 2017; 121: 537–546.
- Zhong H, Tan J, Wang Y, et al. Effects of a diesel particulate filter on emission characteristics of a China II non-road diesel engine. *Energy Fuels* 2017; 31: 9833–9839.
- Bermúdez V, Ruiz S, Conde B and Soto L. Analysis of the aftertreatment performance in HD-SI engine fueled with LPG. *Int J Engine Res*. Epub ahead of print 22 September 2021. DOI: 10.1177/14680874211048138.
- Luján JM, Bermúdez V, Piqueras P and García-Afonso. Experimental assessment of pre-turbo aftertreatment configurations in a single stage turbocharged diesel engine. Part 1: steady-state operation. *Energy* 2015; 80: 599–613.
- Lapuerta M, Rodríguez-Fernández J and Oliva F. Effect of soot accumulation in a diesel particle filter on the combustion process and gaseous emissions. *Energy* 2012; 47: 543–552.
- Serrano JR, Piqueras P, Sanchis EJ and Diesel B. A modelling tool for engine and exhaust aftertreatment performance analysis in altitude operation. *Results Eng* 2019; 4: 100054.
- Boger T, Rose D, Tilgner IC and Heibel AK. Regeneration strategies for an enhanced thermal management of oxide diesel particulate filters. SAE technical paper 2008-01-0328, 2008.
- Tourlonias P and Koltsakis G. Model-based comparative study of Euro 6 diesel aftertreatment concepts, focusing on fuel consumption. *Int J Engine Res* 2011; 12: 238–251.
- Yamada H, Inomata S and Tanimoto H. Mechanisms of increased particle and VOC emissions during DPF active regeneration and practical emissions considering regeneration. *Environ Sci Technol* 2017; 51: 2914–2923.
- Song J, Wang J and Boehman A. The role of fuel-borne catalyst in diesel particulate oxidation behavior. *Combust Flame* 2006; 146: 73–84.
- Luján JM, Guardiola C, Pla B and Reig A. Switching strategy between HP (high pressure)- and LPEGR (low pressure exhaust gas recirculation) systems for reduced fuel consumption and emissions. *Energy* 2015; 90: 1790–1798.
- Joshi A. Progress and outlook on gasoline vehicle after-treatment systems. *Johnson Matthey Technol Rev* 2017; 61(4): 311–325.
- Wang Y, Kamp CJ, Wang Y, et al. The origin, transport, and evolution of ash in engine particulate filters. *Appl Energy* 2020; 263: 114631.
- Millo F, Andreatta M, Rafigh M, Mercuri D and Pozzi C. Impact on vehicle fuel economy of the soot loading on diesel particulate filters made of different substrate materials. *Energy* 2015; 86: 19–30.
- Zhang J, Wong VW, Shuai S, Chen Y and Sappok A. Quantitative estimation of the impact of ash accumulation on diesel particulate filter related fuel penalty for a typical modern on-road heavy-duty diesel engine. *Appl Energy* 2018; 229: 1010–1023.
- Jang J, Lee Y and Kwon O. Comparison of fuel efficiency and exhaust emissions between the aged and new DPF systems of Euro 5 diesel passenger car. *Int J Autom Technol* 2017; 18: 751–758.
- Xiao G, Li B, Tian H, Leng X and Long W. Numerical study on flow and pressure drop characteristics of a novel type asymmetric wall-flow diesel particulate filter. *Fuel* 2020; 267: 117148.
- Wang Y, Pan Y, Su C, Srinivasan A, Gong J and Kamp CJ. Performance of asymmetric particulate filter with soot and ash deposits: analytical solution and its application. *Ind Eng Chem Res* 2018; 57: 15846–15856.
- Belot I, Vidal D, Votsmeier M, Hayes RE and Bertrand F. Numerical investigation of the impact of washcoat distribution on the filtration performance of gasoline particulate filters. *Chem Eng Sci* 2020; 221: 115656.
- Leskovjan M, Němec J, Plachá M, et al. Multiscale modeling and analysis of pressure drop contributions in catalytic filters. *Ind Eng Chem Res* 2021; 60: 6512–6524.
- Allen J. *A method for reducing ash volume in wall-flow diesel particulate filters - water injection as a service tool to improve fuel consumption and particulate filter service life*. MSc Thesis, Linköping University, Sweden, 2017.
- Desantes JM, Payri F, Piqueras P and Serrano JR. Particle filter system for engines and method for reducing pressure loss in said filter. Patent EP2955347, ES2408243, Priority date 11/02/2013.
- Bermúdez V, Serrano JR, Piqueras P and García-Afonso O. Pre-DPF water injection technique for pressure drop control in loaded wall-flow diesel particulate filters. *Appl Energy* 2015; 140: 234–245.
- Serrano JR, Bermúdez V, Piqueras P and Angiolini E. Application of pre-DPF water injection technique for pressure drop limitation. SAE technical paper 2015-01-0985, 2015.

27. Bermúdez V, Serrano JR, Piqueras P and Campos D. Analysis of the influence of pre-DPF water injection technique on pollutants emission. *Energy* 2015; 89: 778–792.
28. Bermúdez V, Serrano J, Piqueras P and Sanchis E. On the impact of particulate matter distribution on pressure drop of wall-flow particulate filters. *Appl Sci* 2017; 7: 234.
29. Du Y, Meng Z, Fang J, et al. Characterization of soot deposition and oxidation process on catalytic diesel particulate filter with ash loading through an optimized visualized method. *Fuel* 2019; 243: 251–261.
30. Fino D, Russo N, Millo F, Vezza DS, Ferrero F and Chianale A. New tool for experimental analysis of diesel particulate filter loading. *Top Catal* 2009; 52: 2083–2087.
31. Serrano JR, Climent H, Piqueras P and Angiolini E. Filtration modelling in wall-flow particulate filters of low soot penetration thickness. *Energy* 2016; 112: 883–898.
32. Serrano JR, Arnau FJ, Piqueras P and García-Afonso Ó. Packed bed of spherical particles approach for pressure drop prediction in wall-flow DPFs (diesel particulate filters) under soot loading conditions. *Energy* 2013; 58: 644–654.
33. Choi S, Oh KC and Lee CB. The effects of filter porosity and flow conditions on soot deposition/oxidation and pressure drop in particulate filters. *Energy* 2014; 77: 327–337.
34. Tan PQ, Wang DY, Yao CJ, et al. Extended filtration model for diesel particulate filter based on diesel particulate matter morphology characteristics. *Fuel* 2020; 277: 118150.
35. Koltsakis G, Konstantinou A, Haralampous O and Samaras Z. Measurement and intra-layer modeling of soot density and permeability in wall-flow filters. SAE technical paper 2006-01-0261, 2006.
36. Sappok A and Wong VW. Lubricant-derived ash properties and their effects on diesel particulate filter pressure-drop performance. *J Eng Gas Turbine Power* 2011; 133: 032805.
37. Sappok A, Govani I, Kamp C, Wang Y and Wong V. In-situ optical analysis of ash formation and transport in diesel particulate filters during active and passive DPF regeneration processes. *SAE Int J Fuel Lubricants* 2013; 6(2): 336–349.
38. Ishizawa T, Yamane H, Satoh H, et al. Investigation into ash loading and its relationship to DPF regeneration method. *SAE Int J Commer Veh* 2009; 2: 164–175.
39. Kamp CJ, Sappok A, Wang Y, Bryk W, Rubin A and Wong V. Direct measurements of soot/ash affinity in the diesel particulate filter by atomic force microscopy and implications for ash accumulation and DPF degradation. *SAE Int J Fuel Lubricants* 2014; 7: 307–316.
40. Zhang J, Li Y, Wong VW, et al. Experimental study of lubricant-derived ash effects on diesel particulate filter performance. *Int J Engine Res* 2021; 22: 921–934.
41. Bollerhoff T, Markomanolakis I and Koltsakis G. Filtration and regeneration modeling for particulate filters with inhomogeneous wall structure. *Catal Today* 2012; 188: 24–31.
42. Zhang B, Zuo H, Huang Z, Tan J and Zuo Q. Endpoint forecast of different diesel-biodiesel soot filtration process in diesel particulate filters considering ash deposition. *Fuel* 2020; 272: 117678.
43. Wang Y, Wong V, Sappok A and Munnis S. The sensitivity of DPF performance to the spatial distribution of ash inside DPF inlet channels. SAE technical paper 2013-01-1584, 2013.
44. Lupše J, Campolo M and Soldati A. Modelling soot deposition and monolith regeneration for optimal design of automotive DPFs. *Chem Eng Sci* 2016; 151: 36–50.